TITLE: Modeling Contrast-to-Noise Ratio from List Mode Reconstructions of ^{68}Ga DOTATATE PET/CT: Predicting Detectability of Hepatic Metastases in Shorter Acquisition PET Reconstructions

AUTHORS:
[1]Michael Silosky, MS
[2]Fuyong Xing, PhD
[1]John Wehrend, MD
[3]Daniel V. Litwiller, PhD
[4]Scott D. Metzler, PhD
[1]Bennett B. Chin, MD

INSTITUTION: University of Colorado School of Medicine Anschutz Medical Campus
[1]Department of Radiology, [2]Department of Biostatistics and Informatics, and [3]GE Healthcare, Denver, CO
[4]Perelman School of Medicine, University of Pennsylvania, Department of Radiology

RUNNING TITLE: Modeling Contrast-to-Noise Ratio from List Mode Reconstructions of 68Ga DOTATATE

CORRESPONDING AUTHOR INFORMATION (address correspondence to):

Michael Silosky, MS
ORCID ID: 0000-0003-3675-5387

University of Colorado Anschutz Medical Campus
Department of Radiology
Division of Radiological Sciences
12401 East 17th Avenue, Mail Stop L954A
Aurora, CO 80045
michael.silosky@cuanschutz.edu
Office Phone number: 303-724-3760
Personal Cell Phone number: 815-302-6156

ARTICLE TYPE: Original research

DECLARATION OF CONFLICT OF INTEREST: None

FUNDING: None

Abstract:

Background:

Deep learning (DL) algorithms have shown promise in identifying and quantifying lesions in PET/CT. However, the accuracy and generalizability of these algorithms relies on large, diverse data sets which are time and labor intensive to curate. Modern PET/CT scanners may acquire data in list mode, allowing for multiple reconstructions of the same data sets with different parameters and imaging times. These reconstructions may provide a wide range of image characteristics to increase the size and diversity of datasets. Training algorithms with shorter imaging times and higher noise properties requires that lesions remain detectable. The purpose of this study is to model and predict the contrast-to-noise ratio (CNR) for shorter imaging times based on CNR from longer duration, lower noise images for ^{68}Ga DOTATATE PET hepatic lesions and identify a threshold above which lesions remain detectable.

Methods:

^{68}Ga DOTATATE subjects (n=20) with hepatic lesions were divided into two subgroups. The "Model" group (n=4 subjects; n=9 lesions; n=36 datapoints) was used to identify the relationship between CNR and imaging time. The "Test" group (n=16 subjects; n=44 lesions; n=176 datapoints) was used to evaluate the prediction provided by the model.

Results:

CNR plotted as a function of imaging time for a subset of identified subjects was very well fit with a quadratic model. For the remaining subjects, the measured CNR showed a very high linear correlation with the predicted CNR for these lesions ($R^2 > 0.97$) for all imaging durations. From the model, a threshold CNR=6.9 at 5-minutes predicted CNR$\geq$5 at 2-minutes. Visual inspection of lesions in 2-minute images with CNR above the threshold in 5-minute images were assessed and rated as a 4 or 5 (probably positive or definitely positive) confirming 100% lesion detectability on the shorter 2-minute PET images.

Conclusions:

CNR for shorter DOTATATE PET imaging times may be accurately predicted using list mode reconstructions of longer acquisitions. A threshold CNR may be applied to longer duration images to ensure lesion detectability of shorter duration reconstructions. This method can aid in the selection of lesions to include in novel data augmentation techniques for deep learning.

Keywords: PET/CT, ^{68}Ga DOTATATE, Artificial Intelligence, Contrast-to-Noise, Detectability

INTRODUCTION

Deep learning (DL) neural networks have demonstrated utility in automatically classifying and quantifying lesions in lymphoma and lung cancer imaging with FDG PET/CT [1, 2]. Excellent results have also been reported in identifying prostate cancer with ^{18}F PSMA PET/CT [3, 4] and ^{68}Ga PSMA PET/CT [5]. Similarly, DL algorithms can be developed to automatically identify hepatic lesions in neuroendocrine tumors with ^{68}Ga DOTATATE [6]. These results are showing potential for improving the speed, accuracy, and reproducibility of DL techniques for identifying and quantifying tumors with PET.

Gastroenteropancreatic neuroendocrine tumors (GEP-NETs), however, are relatively uncommon, and a large number of well-annotated DOTATATE datasets are required to adequately train, validate, and test DL algorithms. Additionally, training datasets with a diversity of noise characteristics are expected to improve the generalizability and performance when tested on real world data; however, this is extremely time and labor intensive to collect. The problem is compounded by the variation in PET scanner performance between generations and models. Modern digital detector PET scanners have substantially higher sensitivity and lower image noise than older models [7]. Consequently, DL algorithms developed using data from new systems may perform poorly on data from other devices.

One approach to aid in addressing this issue would be to use shorter acquisitions from modern systems to simulate noise properties of older scanners. The majority of modern scanners are capable of acquiring data in list mode, at least when acquiring in step-and-shoot mode, and retrospectively reconstructing PET images using shorter acquisition times. This effectively results in higher image noise, similar to older generation analog PET scanners. Additionally, post-reconstruction filtering and device specific reconstruction algorithms may be used to further mimic the behavior of older systems. List mode reconstructions from advanced digital PET cameras, therefore, may increase the size and diversity of the datasets, potentially improving the performance and generalizability of the DL algorithms. List mode generated images from very short acquisition times, however, should have truly detectable lesions in the context of higher image noise. When using list mode to augment the size and diversity of datasets, images should only be degraded to an extent which maintains lesion detectability by human observers.

While many factors influence the detectability of lesions in PET imaging, contrast-to-noise ratio (CNR) is a relatively well validated and commonly used metric. Early studies proposed that that a signal-to-noise ratio “in the neighborhood of 5” provides a reasonable threshold for detection [8]. While a specific threshold for detectability for CNR has been debated, a value of 5 has been utilized in numerous studies and validated as a conservative threshold of lesion detectability [9-11]. Consequently, CNR was selected as the metric of detectability for this study.

The purpose of this study is to determine if the CNR calculated from list mode reconstructions using shorter imaging times can be predicted from the CNR from longer, lower noise images for ^{68}Ga DOTATATE PET hepatic lesions. A secondary objective is to confirm lesion detectability in shorter list mode reconstructions.

METHODS

Phantom Study

Data Acquisition and Reconstruction. To characterize the general relationship between CNR and imaging time, an initial phantom study was performed using a cylindrical phantom with fillable spheres (Data

Spectrum, Durham NC) which was scanned and reconstructed on Discovery MI PET/CT (General Electric, Waukesha, WI) using ^{18}F for 3 minutes in a single bed position. Acquisition time was chosen to mimic clinical ^{18}F scans. Spheres ranged in diameter from 1.5 mm to 15.6 mm. Background activity at scan time was 3.645 kBq/ml corresponding to a nominal background SUV of 1 for a 70 kg patient with an administered activity of 370 MBq (10 mCi) and 1 hour uptake. Sphere activity at the time of scanning was selected to result in a nominal target-to-background ratio of 40 to 1. This ratio was chosen to ensure detectability of the majority of sphere diameters. Data was acquired in list mode and utilized to generate reconstructions with imaging times of 0.25, 0.5, 1.0, 1.5, 2.0, 2.5, and 3.0 minutes using iterative reconstruction (VPFXS) with 3 iterations/16 subsets, a 192 x 192 matrix, 70 cm reconstructed diameter, CT based attenuation correction, and time-of-flight, point spread function recovery, randoms, dead time, scatter, and decay corrections, with a post reconstruction gaussian filter of 5 mm. It should be noted that VPFXS reconstruction is the vendor's trade name for ordered subset expectation maximum (OSEM) reconstruction with point spread function recovery and time-of-flight activated.

CNR Modelling. The CNR at shorter imaging times for the spheres in the phantom study were normalized to the 3-minute CNR. This data was fit with a quadratic function, and based on this data, an analogous procedure was performed for patient hepatic DOTATATE lesions.

Patient study

Patient selection. This study was approved and performed under a waiver of informed consent from our Institutional Review Board. Sequential ^{68}Ga DOTATATE PET/CT scans obtained from a digital detector PET/CT scanner (GE Discovery MI PET/CT, GE Healthcare, Waukesha, WI) were first deidentified, and then screened for hepatic lesion eligibility as previously described [6]. Inclusion criteria included 10 or fewer well defined, non-confluent lesions. The first 20 identified to meet the inclusion criteria were selected for the study resulting in a total of 53 lesions. The selected subjects were divided into two subgroups designated as the "Model" group with 4 subjects (n=9 lesions) and the "Test" group with 16 subjects (n=44 lesions).

Acquisition and reconstruction

For all subjects, clinical ^{68}Ga DOTATATE PET/CT images were acquired used a 5-minute/bed acquisition time and reconstructed using block sequential regularized expectation maximization penalized-likelihood reconstruction algorithm reconstruction (Q.Clear) with a 256 x 256 matrix, 70 cm reconstructed diameter (2.73mm x 2.73mm x 2.79 mm voxel), CT based attenuation correction, and time-of-flight, point spread function recovery, and scatter and decay corrections, (noise penalization factor, BETA=400). Following this standard reconstruction, list mode data was utilized to generate additional reconstructions with imaging times of 2, 3, 4 and 5 minutes using the scanners clinical reconstruction software with iterative reconstruction (VPFXS) with 3 iterations/16 subsets, a 192 x 192 matrix, 70 cm reconstructed diameter, CT based attenuation correction, and time-of-flight, point spread function recovery, and randoms, dead time, scatter and decay corrections, with a post reconstruction gaussian filter of 5 mm.

Liver segmentation and lesion annotation

Hepatic lesions identified as probably or definitely positive on the 5-minute Q.Clear reconstructions were semi-automatically identified and annotated using a customized workflow (MIM version 7.0.3), as previously described (6). Briefly, this process included semi-automated segmentation of the liver,

followed by a semi-automated workflow to identify lesions based on image intensity threshold using modified PERCIST criteria [6] and normal liver background. Lesions were contoured based on gradient edge detection, and then applied to the 2, 3, 4, and 5-minute VPFXS images. Segmentation and annotation were performed on the Q.Clear images with a 5-minute duration since they are our clinical standard and provide high quality images. Quantitative analysis was performed on the VPFXS images of varying durations because, as a form of OSEM reconstruction, the results may be more generalizable. Additionally, because the contours were generated from the gold-standard "Q.Clear" images and then applied to the VPFXS images of varying duration, the segmentation and lesion annotation are consistent and independent of reconstruction method and imaging time."

CNR Calculation and Modeling

For each lesion, CNR was determined by dividing the difference in SUV_{mean} between the lesion and liver background by the standard deviation in the background [12]. To evaluate the effect of shorter imaging time, the CNR determined for 2, 3, and 4-minute images was normalized by dividing by the 5-minute CNR. The mean value and standard deviation of the normalized CNR was calculated for the 2, 3, and 4-minute acquisition times, and plotted as a function of acquisition time. The statistical variation in signal is approximated as the square root of that signal [13], with iterative reconstruction maintaining a similar relationship between CNR and imaging time for detectable lesions as previously shown [14]. Consequently, a quadratic function was selected to model the relative fraction of the 5-minute CNR for shorter imaging times with data fit using a standard least squared regression model in Microsoft Excel (Ver. 16.0).

Model Testing

For the 44 lesions from the "Test" group, the quadratic model was used to predict CNR for the 2, 3, and 4-minute images. Predicted CNR values were plotted as a function of the measured CNR values and fit with linear functions. Additionally, the difference between the predicted and measured CNR was determined for each lesion. Modified Bland-Altman plots were generated with this difference divided by the measured CNR plotted as a function of the measured CNR. Finally, a CNR threshold for the 5-minute VPFXS image was determined from the model, such that the predicted 2-minute CNR would be ≥ 5. To validate the threshold, all lesions with a 5-minute CNR that was above the threshold value were visually inspected on the 2-minute images by a board-certified nuclear medicine physician to verify detectability, determined using the following 5-point Likert scale: No lesion-1; probably negative-2; equivocal-3; probably positive-4; and definitely positive-5.

RESULTS

CNR Modeling

The CNR results for the phantom are shown as a function of imaging time (Fig. 1A) showing a good correlation of data points to the quadratic fit ($R^2 > 0.99$). Following the phantom study, an analysis for ^{68}Ga DOTATATE lesions was similarly performed using a quadratic function as identified in the phantom study. The CNR at shorter imaging times, normalized to the 5-minute CNR, are shown as a function of imaging time for the 9 "Model" lesions (Fig. 1B). This data was also well fit with a quadratic function ($R^2 > 0.99$). On average, the CNR for lesions in 2, 3, and 4-minute images was 72% ± 4%, 85% ± 3%, 95% ± 2% of the CNR in the 5-minute image.

Model Validation

The CNR predicted by the model shown in Fig. 1 was well correlated with measured CNR as shown in Fig. 2. As the imaging time decreased, the error between the prediction and measured values increased. The average difference between predicted and measured values was 13.5%, 6.8%, and 3.4% for 2, 3, and 4-minute image times, respectively. Fig. 3 shows Bland-Altman plots with the difference between the predicted and measured CNR expressed as the absolute difference and as a percentage difference compared to the measured value. The biases were small and only statistically significant for the 2-minute images (-6%) when assessed by the paired t-test (p= 0.001).

CNR Threshold and Visual evaluation

Based on the model shown in Fig. 1, a threshold CNR of approximately 6.9 in the 5-minute images was predicted to result in a CNR of approximately 5 in the 2-minute images. All lesions with a CNR ≥ 6.9 (n = 23) in the 5-minute images were assessed and rated as a 4 (probably positive; n =2) or 5 (definitely positive; n = 21) confirming 100% lesion detectability on the shorter reconstruction 2-minute images.

A representative detectable lesion with low CNR = 2.9 on the 5-minute image shows that decreasing the time to 2 minutes results in sufficiently high noise to make the lesions difficult to identify from the background noise (Fig. 4), and high image noise could potentially be misinterpreted as a small lesion. A representative lesion with a high CNR = 6.6 on the 5-minute image is definitely positive on the 2-minute image, despite being slightly below the threshold of 5 (Fig. 5; CNR = 4.6;). Another similarly high CNR = 6.8 lesion at 5-minutes is definitely positive on the 2-minute image with measured CNR =5.6 (Fig. 6).

DISCUSSION

This study demonstrates the feasibility of modeling and predicting the CNR of noisier, shorter acquisition ^{68}Ga DOTATATE PET hepatic lesions from longer acquisition, list mode reconstructions. As expected, the variability of predicted CNR increases as the imaging time decreases, and this is highest for the 2-minute images. This predicted CNR at 2-minutes, however, remains well correlated with the measured values. This data also demonstrates that a CNR threshold may be applied to images with longer acquisition times to control the minimum CNR of lesions when reconstructed with shorter times and help ensure detectability. All lesions identified above the threshold CNR of 6.9 in the 5-minute images were detectable on the 2-minute images.

The overall goal of this study is to facilitate the development of data augmentation techniques to assist in training of DL algorithms for automated lesion detection. List mode reconstructions from advanced digital PET could enrich the training data set with images from a wider range of noise properties, and they also increase the number of annotated datasets by several fold with minimal additional effort. The modeling procedure performed in this study provides a method to identify candidate lesions such that the noisier, shorter acquisition, degraded images will remain detectable and appropriate for use in training of the DL algorithms. Further work is required to test the performance of DL algorithms trained with and without this data augmentation technique.

In addition to DL applications, list mode reconstructions have been used to aid in clinical protocol development. To evaluate the potential for reduced imaging time or reduced imaging dose for ^{68}Ga PSMA PET / CT, an observer study evaluating lesion detectability and image quality was performed [15]. This study did not find evidence for potentially lowering the administered dose while maintaining image

quality and lesion detectability. This study, however, was limited to the evaluation of only 11 subjects and 21 lesions using an analog crystal detector PET/CT system with lower sensitivity compared to advanced digital detector PET/CT.

Similarly, a clinically relevant, combined phantom and patient study of ^{68}Ga PSMA PET/CT used list mode reconstructions to determine if reduced imaging time or administered dose could maintain lesion detectability and quantitative accuracy [14]. Using the criteria of maintaining CNR ≥ 5, and a percentage difference of SUV_{max} ≤ 20%, a short 140-second list mode reconstruction preserved all lesion detectability and SUV max measurements using a threshold of mean lesion COV of 25%. Using these criteria, this study concluded that reducing the imaging time from 240 to 140 seconds per bed position was acceptable while maintaining a CNR $\geq$ 5. These apparently conflicting results emphasize the complexity of determining appropriate imaging time and dose in clinical practice due to the specific characteristics of the radiotracer, lesion uptake, lesion size, background, background noise characteristics, reconstruction techniques, and PET scanner sensitivity [11, 16].

While CNR provides a relatively straightforward metric for estimating lesion detectability, identifying the lowest discrete threshold above which all lesions remain detectable on shorter acquisition list mode reconstructions was not performed in this study. The threshold value of 5 has been used in several previous studies, with a reference a range of 3 to 5 previously reported using an analytical method [17]. Concordant with this, list mode reconstructions of ^{68}Ga PSMA PET / CT reported lesion detectability as low as CNR = 3.8 [14]. Similarly, our study was concordant with lesion detectability using CNR $\geq$ 5, with some 2-minute images remaining clearly visible below this threshold (Fig. 5). The purpose of this study was to ensure operator detectability was maintained above a specified CNR ratio, and thus, the threshold of 5 for 2-minute PET images was chosen as a relatively conservative assumption. For larger targets or images with different noise characteristics, a lower threshold may be reasonable. As new radiotracers are developed, a CNR model could assist in specific protocol development to maintain lesion detectability for specific PET systems.

This work has demonstrated the feasibility of predicting CNR for shorter acquisition time images, however, some limitations may affect its generalizability. First, the total number of subjects (n=20), individual lesions (n=53), and total time datapoints (n=212) in this study is relatively modest. The accuracy of the CNR model, therefore, is limited to this dataset, but could improve with a larger sample size. Secondly, this study is limited to a single radiopharmaceutical with specific reconstruction parameters on a single PET scanner and limited to a single organ. Although the general relationship between imaging time and CNR should be broadly applicable to other radiotracers, PET systems, and other organs, this feasibility study did not attempt to validate the generalizability. The specific fit parameters in the model are also likely to be different for specific radiotracers, PET scanners, and acquisition and reconstruction techniques. List mode acquisitions from advanced digital PET scanners, however, are capable of reconstructing images with lower spatial resolution, and without advanced correction techniques e.g., depth dependent resolution recovery or high temporal resolution time-of-flight to simulate data from older generation cameras. Finally, lesion detectability was not prospectively validated by human observers. Our study chose a relatively high threshold of CNR to define the threshold of lesion detectability based on Rose's criteria, validated in prior reports. Lesion detectability can be complex and influenced by other factors such as the size and appearance of the lesion, and thus, prospectively validating lesion detectability and generalizability are needed in future studies. Despite these limitations, further validation of this technique could provide a powerful tool to assist DL algorithm development by increasing the number and diversity of the datasets used for DL training in lesion detection.

CONCLUSION

List mode reconstructions provide CNR estimates which show good correlation with measured CNR. Visual evaluation of lesions on 2-minute images verified that those lesions were clearly detectable based on the CNR threshold of 6.9 on the high count, 5-minute images. This data confirms that CNR may be accurately predicted for hepatic lesions on shorter 2-minute acquisitions, and thus, this provides an estimate of a lower limit of lesion detectability. This method can aid in guiding the selection of lesions to include in novel data augmentation techniques for deep learning.

References:

[1] Sibille L, Seifert R, Avramovic N, Vehren T, Spottiswoode B, Zuehlsdorff S, et al. (18)F-FDG PET/CT Uptake Classification in Lymphoma and Lung Cancer by Using Deep Convolutional Neural Networks. Radiology. 2020;294(2):445-52.

[2] Weisman AJ, Kim J, Lee I, McCarten KM, Kessel S, Schwartz CL, et al. Automated quantification of baseline imaging PET metrics on FDG PET/CT images of pediatric Hodgkin lymphoma patients. EJNMMI Physics. 2020;7(1):76.

[3] Nickols N, Anand A, Johnsson K, Brynolfsson J, Borreli P, Parikh N, et al. aPROMISE: A Novel Automated PROMISE Platform to Standardize Evaluation of Tumor Burden in (18)F-DCFPyL Images of Veterans with Prostate Cancer. Journal of Nuclear Medicine. 2022;63(2):233-9.

[4] Johnsson K, Brynolfsson J, Sahlstedt H, Nickols NG, Rettig M, Probst S, et al. Analytical performance of aPROMISE: automated anatomic contextualization, detection, and quantification of [(18)F]DCFPyL (PSMA) imaging for standardized reporting. European Journal of Nuclear Medicine and Molecular imaging. 2021. 2022 Feb;49(3):1041-1051.

[5] Zhao Y, Gafita A, Vollnberg B, Tetteh G, Haupt F, Afshar-Oromieh A, et al. Deep neural network for automatic characterization of lesions on 68Ga-PSMA-11 PET/CT. European Journal of Nuclear Medicine and Molecular Imaging. 2020;47(3):603-13.

[6] Wehrend J, Silosky M, Xing F, Chin BB. Automated liver lesion detection in (68)Ga DOTATATE PET/CT using a deep fully convolutional neural network. EJNMMI research. 2021;11(1):98.

[7] Koopman D, van Dalen JA, Stevens H, Slump CH, Knollema S, Jager PL. Performance of Digital PET Compared with High-Resolution Conventional PET in Patients with Cancer. Journal of Nuclear Medicine. 2020;61(10):1448-54.

[8] Burgess A. The Rose model, revisited. J Opt Soc AM A Opt Image Sci Vis. 1999;16:633-46.

[9] Adler S, Seidel J, Choyke P, Knopp MV, Binzel K, Zhang J, et al. Minimum lesion detectability as a measure of PET system performance. EJNMMI physics. 2017;4(1):1-14.

[10] Silosky M, Karki R, Chin B. 68Ga and 18F quantification, and detectability of hot spots using an ACR Phantom: Contributions of radionuclide physical differences to hot spot detectability. Journal of Nuclear Medicine. 2019;60(supplement 1):1200.

[11] Silosky MS, Karki R, Morgan R, Anderson J, Chin BB. Physical characteristics of (68)Ga DOTATATE PET/CT affecting small lesion detectability. American journal of nuclear medicine and molecular imaging. 2021;11(1):27-39.

[12] Bushberg JS, JA; Leidholdt, E; Boone, J The Essential Physics of Medical Imaging. 3rd ed: Lippincott Williams and Wilkins; 2011.

[13] Cherry SR SJ, Phelps ME. Physics in Nuclear Medicine. 3rd ed. Philadelphia: Elsevier/Saunders; 1980.

[14] Wielaard J, Habraken JBA, Brinks P, Lavalaye J, Boellaard R. Optimization of injected (68)Ga-PSMA activity based on list-mode phantom data and clinical validation. EJNMMI Physics. 2020;7(1):20.

[15] Rauscher I, Fendler WP, Hope TA, Quon A, Nekolla SG, Calais J, et al. Can the Injected Dose Be Reduced in 68Ga-PSMA-11 PET/CT While Maintaining High Image Quality for Lesion Detection? Journal of Nuclear Medicine. 2020;61(2):189-93.

[16] Silosky MS, Patten LW, Chin BB. Small target repeatability of (68)Ga and (18)F: effects of target concentration and imaging time on SUV measurements in clinically relevant phantoms. American journal of nuclear medicine and molecular imaging. 2021;11(4):280-9.

[17.] Bao Q, Chatziioannou AF. Estimation of the minimum detectable activity of preclinical PET imaging systems with an analytical method. Medical physics. 2010;37(11):6070-83.

Figures:

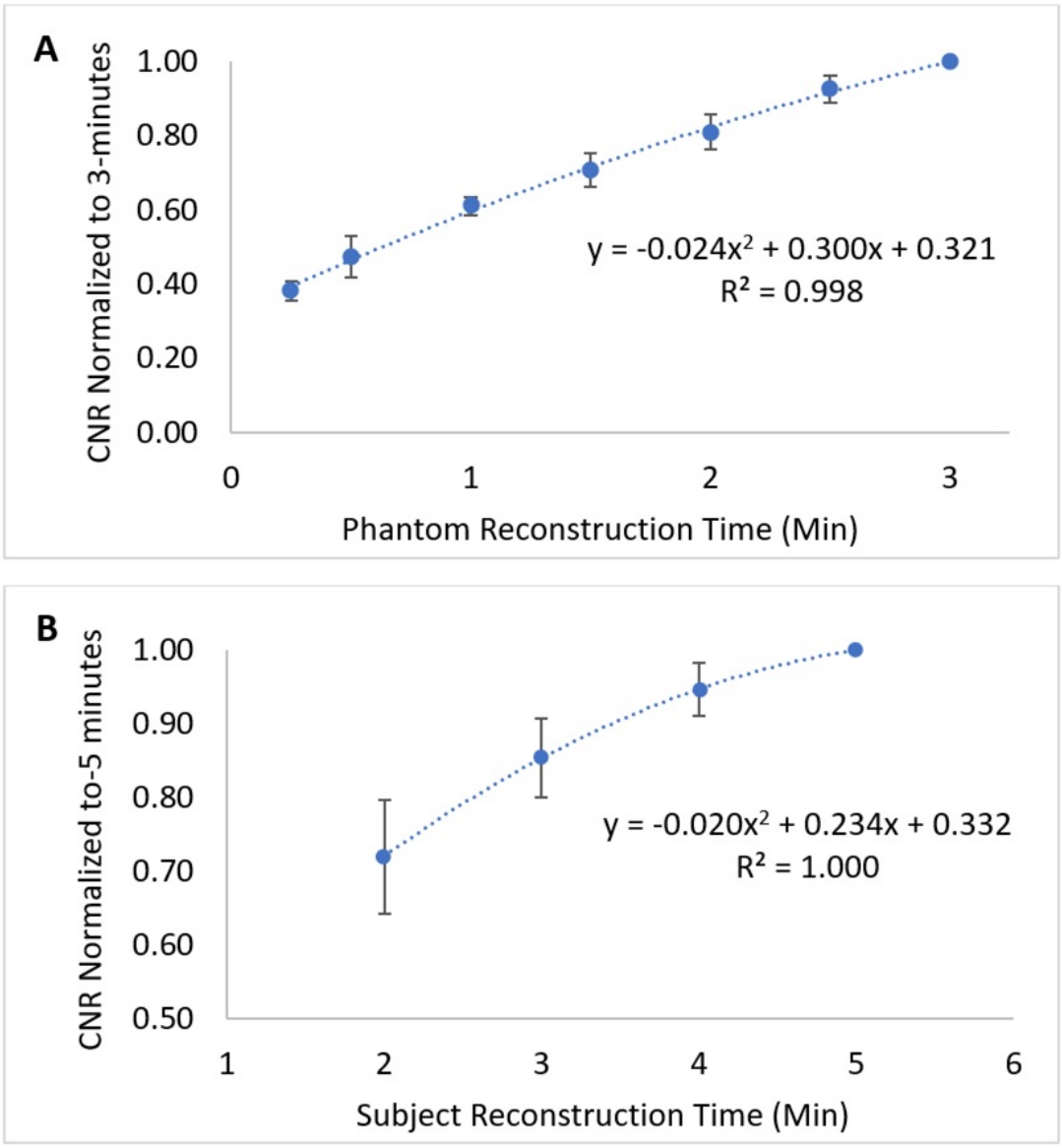

Fig. 1: CNR as a function of time for A) phantom data timepoints normalized to the 3-minute baseline acquisition, and B) subject data (2, 3, and 4-minutes; n=9 different model lesions) normalized to the 5-minute baseline CNR acquisition. Mean values are plotted as a function of acquisition time. These values are well-fit with a quadratic function in both experiments. Error bars represent 2 standard deviations for both sets of data to approximate the 95% confidence interval.

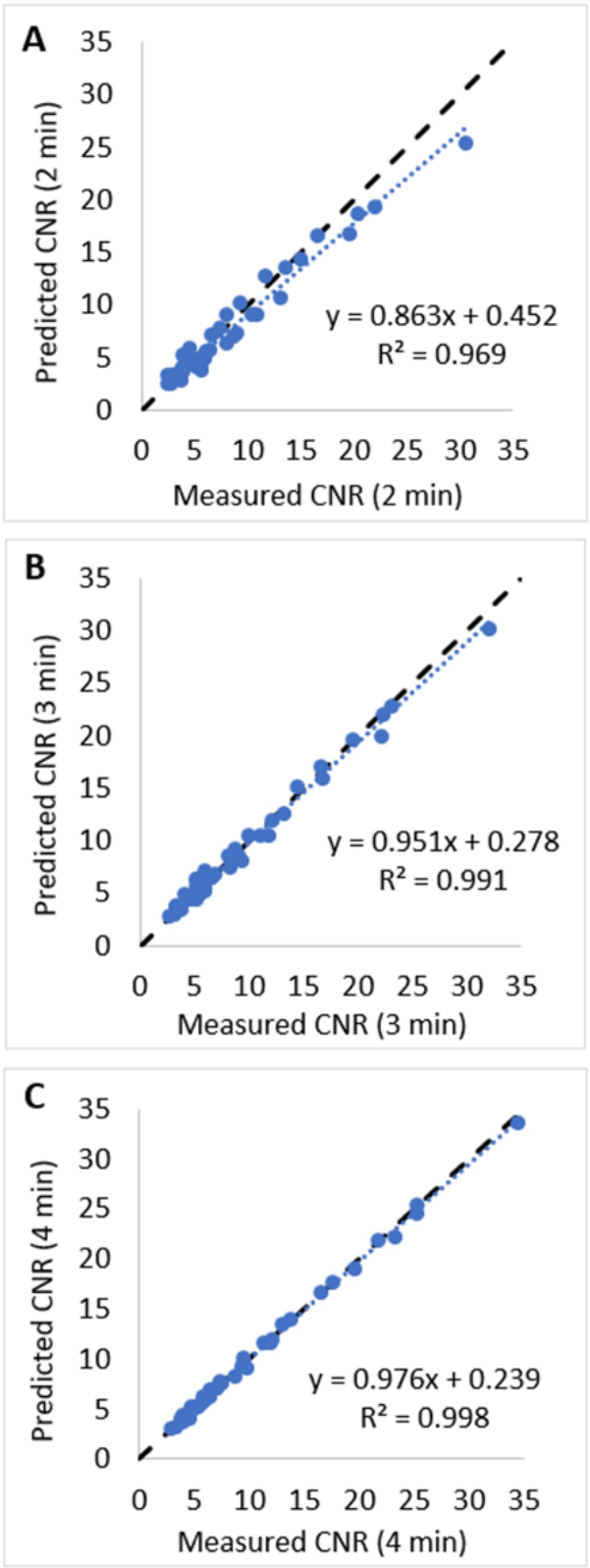

Fig. 2: Measured versus predicted CNR based on the model in Fig. 1B. CNR for each of the 44 "Test" lesions at (A) 2-minutes, (B) 3-minutes, and (C) 4-minutes. Predicted CNR showed a very high linear correlation with measured CNR lesions ($R^2 \geq 0.97$). The black, dashed line represents perfect correlation.

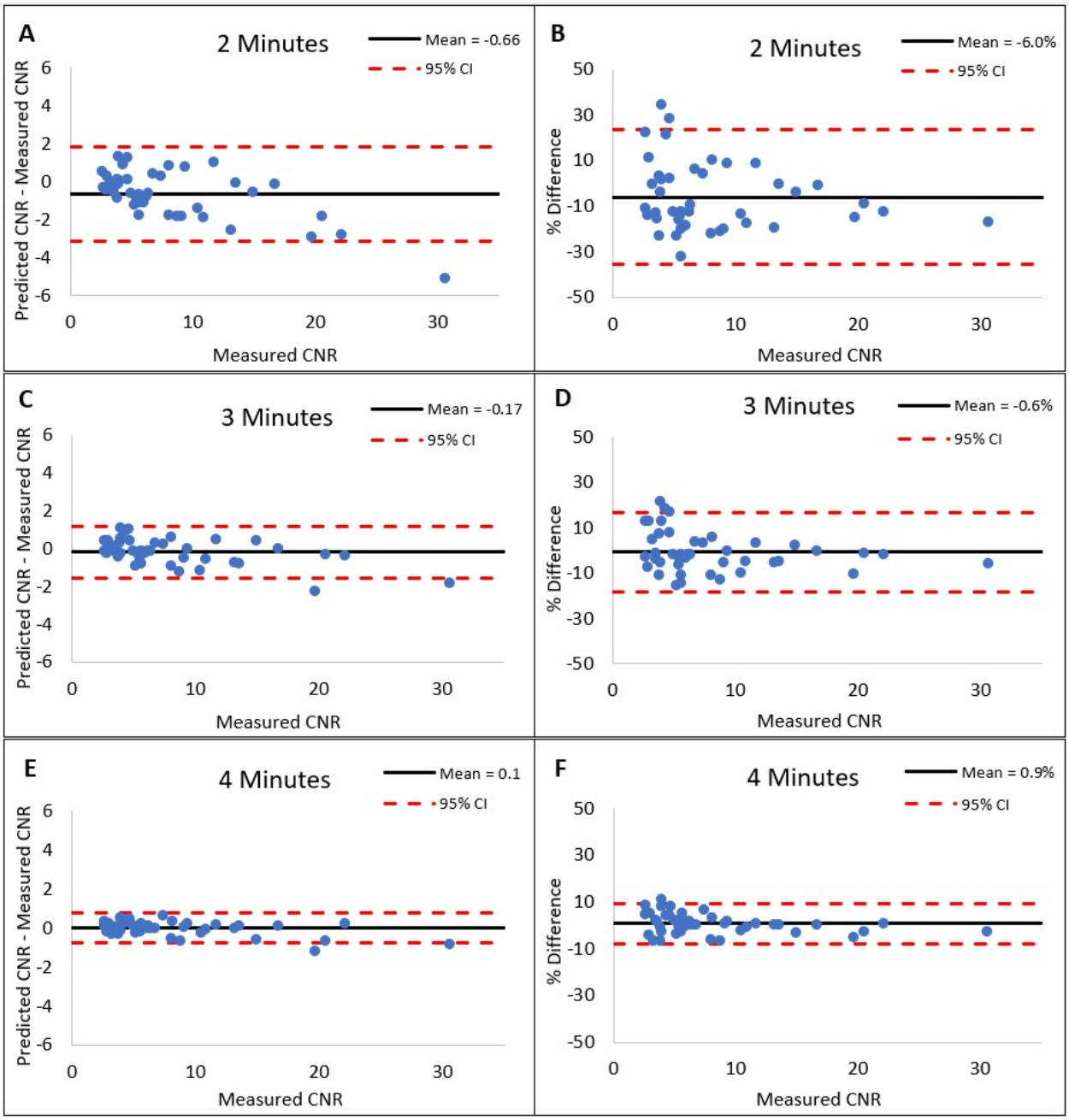

Fig. 3: Bland-Altman plots of the difference between measured and predicted CNR. (Left column) Absolute difference; (right column) percentage difference. CNR for (A, B) 2-minute; (C, D) 3-minute; (E, F) 4-minute imaging. The solid black line represents the mean difference; red dashed lines are 2 standard deviations, estimating the 95% confidence interval. Bias in the 2-minute plot was small, -6% (paired t-test P = 0.001). Bias in the 3 and 4-minute images was less than 1% and not statistically significant (P = 0.11, 0.92, respectively).

Figure 4

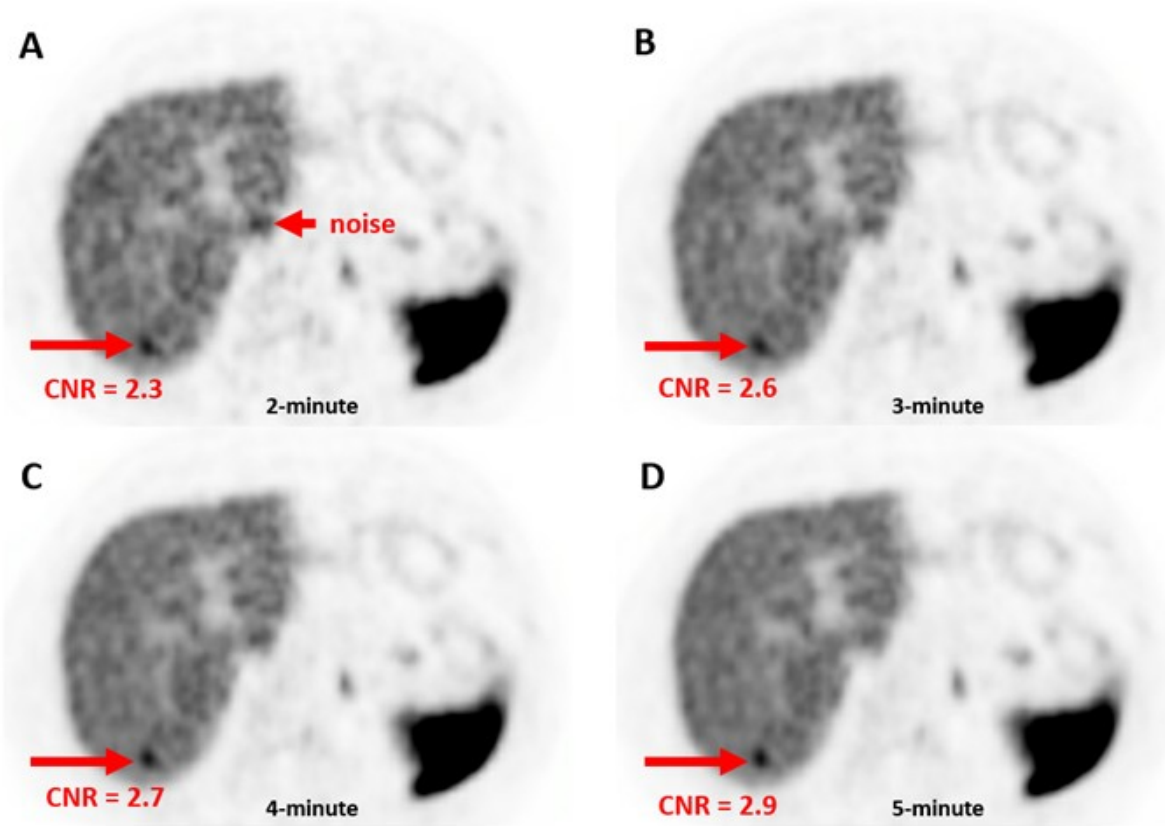

Fig. 4: ^{68}Ga DOTATATE PET transaxial slices with several different list mode reconstruction times. Red arrow (long arrow) shows lesion with baseline 5-minute CNR= 2.9. Background noise (short arrow) difficult to distinguish from true lesion. A) 2-minutes, CNR measured=2.3; B) 3-minutes, CNR measured= 2.6; D) 4-minutes, CNR measured=2.7; D) 5-minutes, CNR measured=2.9. Lesion SUV mean=9.9. All images are scaled with upper threshold SUV=15.

Figure 5

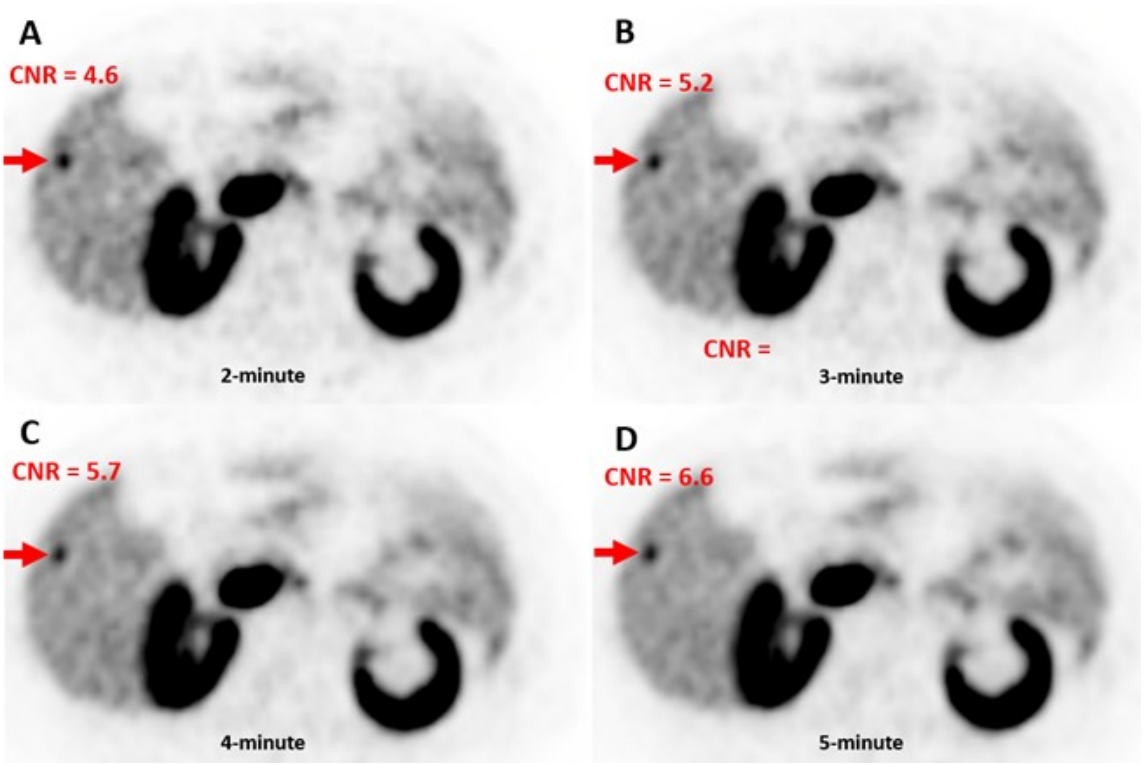

Fig. 5: ^{68}Ga DOTATATE PET transaxial slices with several different list mode reconstruction times. Red arrow shows lesion with baseline 5-minute CNR=6.6. At 2-minutes, lesion is distinguishable from background noise. A) 2-minutes, CNR measured=4.6; B) 3-minutes, CNR measured=5.2; D) 4-minutes, CNR measured=5.7; D) 5-minutes, CNR measured=6.6. All images are scaled with upper threshold SUV=10.

Figure 6

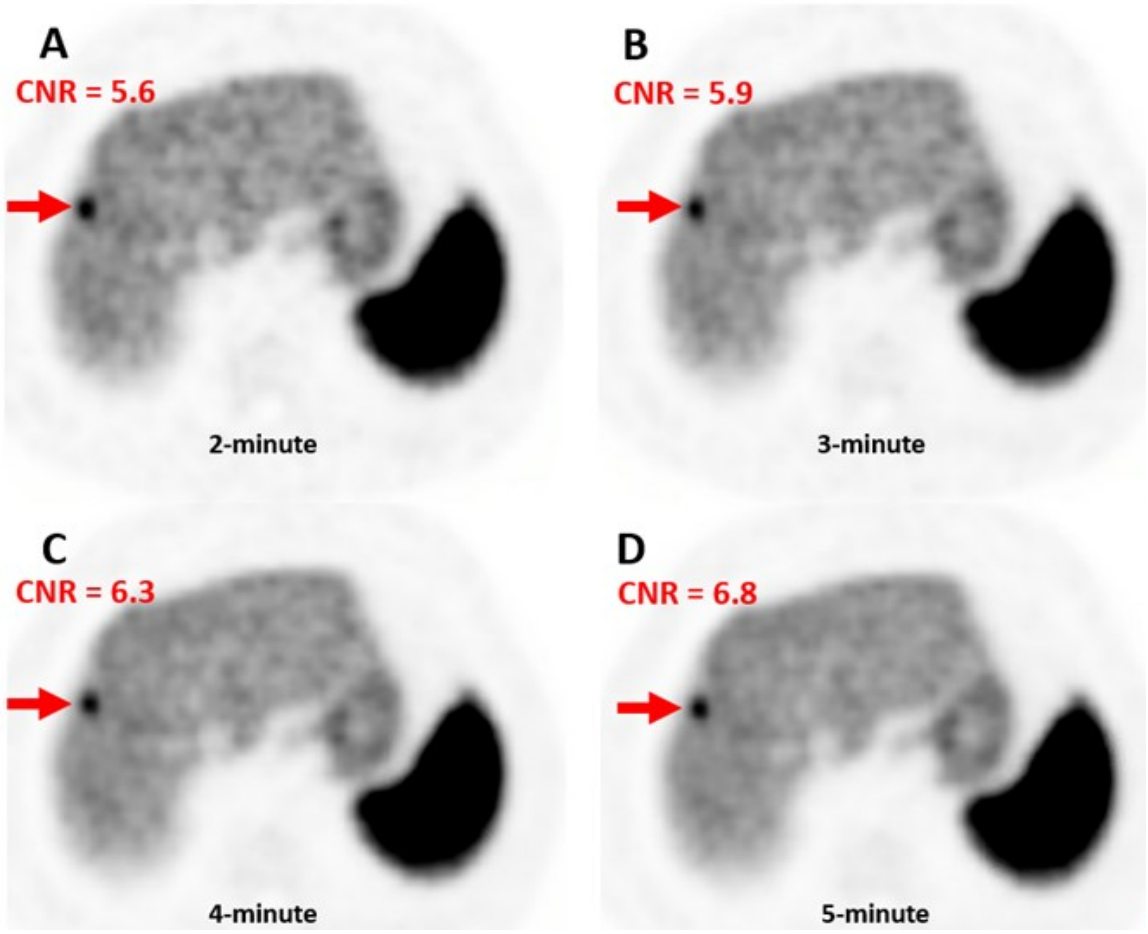

Fig. 6: ^{68}Ga DOTATATE PET transaxial slices with several different list mode reconstruction times. Red arrow shows lesion with baseline 5-minute CNR= 6.8. At 2-minutes, lesion is clearly distinguishable from background noise. A) 2-minutes, CNR measured=5.6; B) 3-minutes, CNR measured=5.9; D) 4-minutes, CNR measured=6.3; D) 5-minutes, CNR measured= 6.8. All images are scaled with upper threshold SUV = 15.